collections of SiC particles. Thus, our calculated ^{22}Na/^{23}Na atmospheric ratio may not be quite adequate for those rich carriers. Our model also does not yet explain naturally why the fraction of particles rich in ^{22}Ne is also rich in ^{4}He. That correlation does seem natural in the model (*5*, *6*) based on a wind from the He shell in a low-mass AGB star, whose shell is not hot enough to burn the ^{22}Ne that exists there (*4*). The latter model, on the other hand, has not accounted for the Si compositions of the particles. Thus, problems in interpretation abound for these competing pictures.

Because the ^{22}Na-bearing particles are formed at a special epoch in the star's evolution (the onset of the "superwind phase"), further correlations or anticorrelations between Ne-E content and other isotopes become plausible. In addition, the ^{22}Na interpretation required by our model may be correct even if some other explanation for the Si-isotope correlation can be found. We especially note that almost one-third of the large graphite particles in the residues carry an even purer form of Ne-E (*7*) without the accompanying ^{4}He (*20*). These particles may also find natural interpretations in the ^{22}Na production scheme because the C star atmospheres have tenfold more C than Si and should therefore also condense graphite. The graphite simply lacks the Si diagnostic (unless Si can be detected as a trace element in those particles).

Our approach is not to seek the most plausible explanation of the noble gas contents of the SiC particles. Rather, we explore the implications for Ne and other noble gases of a specific theoretical model that can account for the Si isotopes. After all, the particles are built of Si. To constrain this model, new work is needed. The Na concentration in the large particles must be measured so that their implied ^{22}Na/^{23}Na ratio can be accurately inferred. Other isotopic clues must also be interpreted. Foremost among these is the puzzling variation of the ^{13}C/^{12}C ratio, which is strongly impacted by the same hot bottom burning that creates the ^{22}Na. The crucial clue of Ne-E has been reinterpreted in terms of the old suggestion (*8*) of ^{22}Na parentage in stellar outflows, which describes it as an extinct radioactivity. This success ties the massive AGB star picture (*13*) to more data. Another puzzle is why only massive AGB stars have made the large SiC particles when low-mass AGB stars are more numerous. It is not clear whether a single nearby massive AGB star has produced all of these presolar particles and injected them into the placental solar cloud, as Cameron (*21*) advocates for other reasons. Another possibility is that only massive AGB stars are able to nucleate and grow the large SiC particles, as we (*13*) advocate. In the former case the data describe details of the formation of the sun and of that particular AGB star (*21*). In the latter case, they describe a general interstellar aspect of "cosmic chemical memory" (*22*) and of the entire spectrum of AGB star evolution.

REFERENCES AND NOTES

1. B. Srinivasan and E. Anders, *Science* **201**, 51 (1978).
2. D. D. Clayton and R. A. Ward, *Astrophys. J.* **224**, 1000 (1978).
3. M. Tang and E. Anders, *Geochim. Cosmochim. Acta* **52**, 1235 (1988).
4. I. Iben, *Q. J. R. Astron. Soc.* **26**, 1 (1985).
5. R. S. Lewis *et al.*, *Nature* **348**, 293 (1990).
6. R. Gallino *et al.*, *ibid.*, p. 298.
7. The largest 3- to 5-μm SiC particles have ^{20}Ne/^{22}Ne ratios as small as 0.1 (*5*), in stark contrast to atmospheric or solar ratios near 13. Low-mass AGB He shells are also rich in ^{22}Ne (*4, 5*), which leads to the suggestion (*5, 6*) that implantation of a terminal AGB wind from the He shell could be the source of Ne-E. The Ne-E in the SiC particles is called Ne-E(H) in meteoritics literature to distinguish it from the Ne-E(L) in graphite particles. The letters H and L refer to high- and low-density separates of the carbonaceous residues. The Ne-E(L) in graphite is even more purely ^{22}Ne, with ^{20}Ne/^{22}Ne as low as 0.01.
8. D. D. Clayton, *Nature* **257**, 36 (1975).
9. E. K. Zinner, M. Tang, E. Anders, *Geochim. Cosmochim. Acta* **53**, 3273 (1989).
10. J. Stone, I. D. Hutcheon, S. Epstein, G. J. Wasserburg, *Earth Planet. Sci. Lett.* **107**, 570 (1991).
11. A. Virag *et al.*, *Geochim. Cosmochim. Acta* **56**, 1715 (1992).
12. M. Obradovic, L. E. Brown, S. Guha, D. D. Clayton, *Meteoritics* **26**, 381 (1991).
13. L. E. Brown and D. D. Clayton, *Astrophys. J.* **392**, L79 (1992).
14. G. Bazan, thesis, University of Illinois (1991).
15. In pulsed reactions followed repeatedly by remixture with solar composition material, the shell composition relaxes asymptotically to a nearly constant makeup, usually in a few pulses. This is commonly called saturation.
16. L. E. Brown and D. D. Clayton, in preparation.
17. M. Frenklach, C. S. Carmer, E. D. Feigelson, *Nature* **339**, 196 (1989).
18. G. R. Caughlan and W. A. Fowler, *At. Data Nucl. Data Tables* **40**, 283 (1988).
19. S. Amari, P. Hoppe, E. Zinner, R. S. Lewis, *Meteoritics* **27**, 197 (1992).
20. R. H. Nichols, Jr., *et al.*, *Lunar Planet. Sci.* **23**, 989 (1992).
21. A. G. W. Cameron, in *Protostars and Planets III*, E. Levy, J. Lunine, M. Matthews, Eds. (Univ. of Arizona Press, Tucson, 1992), pp. 44–73.
22. D. D. Clayton, *Q. J. R. Astron. Soc.* **23**, 174 (1982).
23. We thank R. H. Nichols, Jr., and E. K. Zinner for discussions of their data before publication. We thank I. Iben, Jr., for the use of his envelope code and G. Bazan for several aspects of its implementation. Supported by the National Aeronautics and Space Administration under the Planetary Materials and Geochemistry Program and the Origins of Solar Systems Program.

19 June 1992; accepted 27 August 1992

Chemical Contrast in X-ray Microscopy and Spatially Resolved XANES Spectroscopy of Organic Specimens

H. Ade,* X. Zhang, S. Cameron, C. Costello, J. Kirz, S. Williams

The scanning transmission x-ray microscope at the National Synchrotron Light Source has been used to record x-ray absorption near-edge structure (XANES) spectra from 0.01-square-micrometer regions of organic specimens. The spectral features observed reflect the molecular structure of the dominant absorbing atoms and provide the contrast mechanism for high-resolution imaging with chemical sensitivity. This technique was used with x-ray energies near the carbon *K* absorption edge to identify and map separate phases in various polymer blends and to map the DNA distribution in chromosomes with a spatial resolution of 55 nanometers.

Although electron microscopy is a standard technique for high-resolution imaging of organic specimens and electron energy loss spectroscopy (EELS) is frequently used to obtain chemical information at reduced spatial resolution, radiation damage poses serious limitations for methods that use electron beams (*1*). Recent work in x-ray absorption spectroscopy by Kirtley *et al.* (*2*) indicates that resonance structures near the *K* shell absorption edge of nitrogen provide a means to differentiate chemical species such as DNA and protein. These authors suggest that this resonance structure should provide a good contrast mechanism for bond-specific x-ray imaging. Their observation confirms earlier suggestions by Solem and Baldwin (*3*) and by Solem and Chapline (*4*) that near-edge resonances of nitrogen could be exploited in biological x-ray microscopy.

In this report, we present evidence that an analogous contrast mechanism exists in the x-ray absorption near-edge structure of

---

H. Ade, X. Zhang, J. Kirz, S. Williams, Department of Physics, State University of New York at Stony Brook, Stony Brook, NY 11794.
S. Cameron and C. Costello, EXXON Research and Engineering, Route 22, Annandale, NJ 08801.

*To whom correspondence should be addressed at Department of Physics, North Carolina State University, Box 8202, Raleigh, NC 27695.

carbon (C-XANES) (5). We acquired C-XANES spectra from sample areas as small as 0.01 μm^2 and showed that x-ray micrographs with a resolution of 55 nm indeed exhibit the expected sharp chemical differentiation. We demonstrated the technique on polymer blends and on freeze-dried chromosomes of the bean *Vicia faba*, showing that at least in these systems, radiation damage does not interfere with the investigations.

We used for this work the scanning transmission x-ray microscope (STXM) at the National Synchrotron Light Source. The wavelength of the x-ray beam is selected by a spherical-grating monochromator, with a bandwidth of 0.006 nm for a 100-μm exit slit typically used (6). This corresponds to energy widths of about 0.4, 0.8, and 1.7 eV at photon energies of 290, 405, and 540 eV, respectively. One can adjust the energy width by changing the slit size. A phase zone plate (7) is used to focus the beam to a microprobe, the size of which determines the spatial resolution. The microscope has been well characterized, and a Rayleigh resolution of 55 nm has been measured (8). The specimen is mechanically scanned under computer control, and transmitted x-rays are detected with the use of a gas flow counter. The microscope operates in a helium atmosphere, separated from the beamline vacuum by a 120-nm-thick silicon nitride membrane. Because images are acquired and stored in digital form, they lend themselves naturally to direct measurement and quantitative analysis of the specimen absorptivity at each pixel. For our work, new capabilities were added: (i) operation of the STXM in previously inaccessible photon energy ranges between 285 and 340, 405 and 460, and 530 and 590 eV, which allowed us to obtain carbon, nitrogen, and oxygen XANES spectra and (ii) the recording of XANES spectra in situ from small areas. During acquisition of spectra, the scanning stage is held fixed, while the monochromator grating is scanned in synchrony with the focusing adjustment. This combined motion is necessary to keep the target in focus, because the focal length of the zone plate is proportional to the x-ray energy. A typical spectrum with 500 data points is recorded in about 5 s (Fig. 1). Spectra can be acquired from areas 0.01 μm^2 in size (9) and were corrected for structure in the incident beam intensity caused by carbon and nitrogen on the optical surfaces and in the silicon nitride membranes used as vacuum window, zone plate support, and counter window. These membranes presently limit the usable N-XANES region because they attenuate the beam too much between 400 and 405 eV for reliable data acquisition. Although we recorded spectra and images near the N edge as well as the O edge, the data presented here are restricted to the C edge.

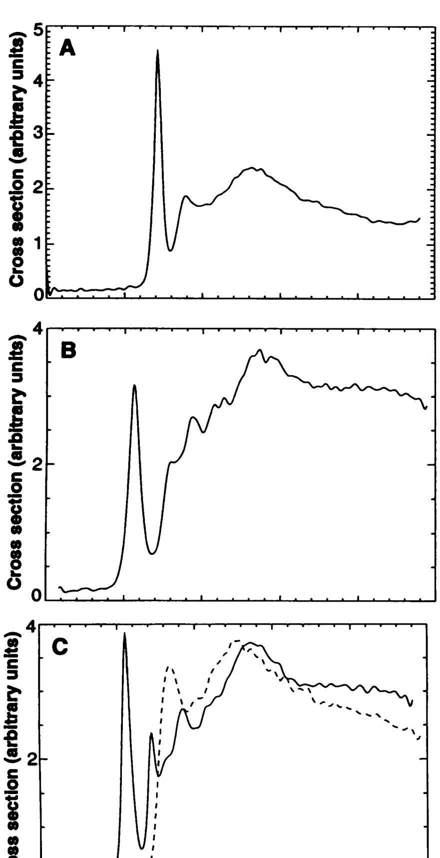

Fig. 1. Carbon *K* shell XANES spectra of (**A**) polyacrylonitrile, (**B**) polystyrene, and (**C**) polypropylene (dashed line) and a 50-50 percent by weight random copolymer of polystyrene and acrylonitrile (solid line). The spectrum in (B) is from a single-phase standard under normal, in-focus operating conditions, whereas all the other spectra were acquired with the STXM from inhomogeneous samples as presented in Figs. 2 and 3. The size of the areas probed is about 0.01 μm^2 (9). Acquisition time was 5 s. All spectra were high-pass filtered in the Fourier domain (17).

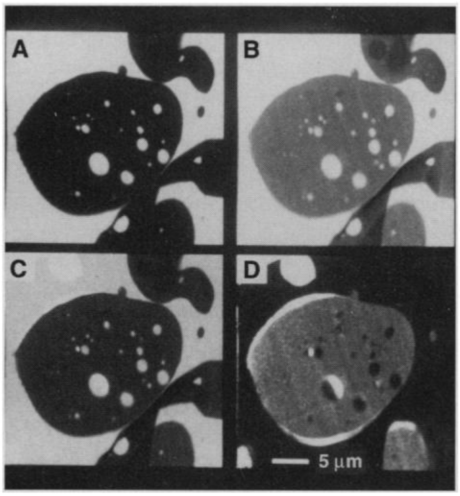

Fig. 2. Images of a 0.5-μm-thick section of a blend consisting of polypropylene and a 50-50 percent by weight random styrene-acrylonitrile copolymer at the following photon energies: (**A**) 285.5 eV, (**B**) 286.2 eV, (**C**) 286.8 eV, and (**D**) 287.9 eV. The contrast arises from differences in the near-edge absorption cross section of the different domains as shown in Fig. 1C. The black (B) and white (W) levels of the micrographs are individually adjusted, with the levels referenced to the incident intensity I_0 as follows: (A), (B), and (C), W = I_0, B = 0; (D), W = 0.3 × I_0, B = 0 (300 × 300 pixels, 2 ms per pixel).

C-XANES spectra of polystyrene, polyacrylonitrile, and polypropylene and a 50-50 percent by weight copolymer of styrene and acrylonitrile were acquired with the STXM at an energy resolution of 0.4 eV (Fig. 1). Spectral differences are clearly visible and related to the presence or absence of various functional groups, such as benzene (sp^2 hybridization) or nitrile (sp hybridization). We used these differences in absorption cross section to provide image contrast in various blends of these polymers, to determine the morphology of these blends, and to identify the composition of the various phases. The micrographs in Fig. 2 represent images of a 0.5-μm-thick section of a blend of polypropylene with a random 50-50 percent by weight copolymer of styrene and acrylonitrile. Domains that corresponded to two phases are clearly identifiable. Note that in the case of Fig. 2A, at a photon energy of 285.5 eV the contrast is almost 100%, whereas at 287.9 eV (Fig. 2D) contrast is reversed. In Fig. 2, A and C, the styrene-acrylonitrile copolymer indeed forms a single phase as expected. The high absorption in Fig. 2A is a result of the antibonding π orbital (π*) resonance of styrene; in Fig. 2C, it is a result of the π* resonance of acrylonitrile. Besides the domains various other features, such as holes and two smaller pieces of an additional layer of polymer film, can be identified. The adhesion between the domains appears to be poor because several interfaces separated during sectioning.

Additional micrographs (Fig. 3) were acquired of a blend that consisted of polypropylene and polystyrene and a small amount of a substance (a compatibilizer) that ensures good adhesion at the interface (no separation during sectioning was encountered) and generally leads to smaller domain sizes. This blend, in contrast to the one in Fig. 1, did not exhibit inclusions of the matrix polymer in the polystyrene domains.

The importance of these images to polymer science lies in the fact that they were obtained with chemical specificity and that the sample was not altered by beam damage or aggressive staining techniques. Information concerning domain size, presence of inclusions, and interparticle distance is important with respect to polymer blend mechanical properties. The relation between morphology and the mechanical properties of rubber-filled polymer blends has been the subject of much work (*10, 11*). In particular, the interparticle distance between rubber domains in a polymer matrix has been shown to be the critical morphological parameter that correlates the ductile-to-brittle transition with the rubber content and rubber particle size (*12*).

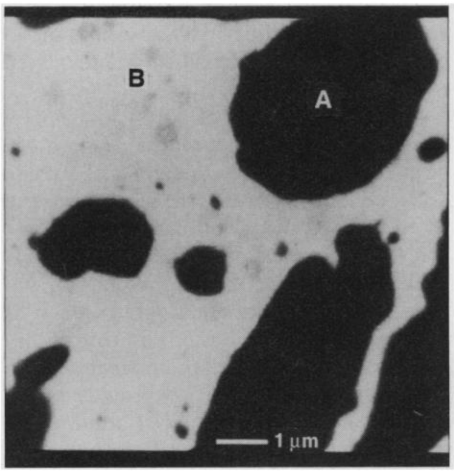

Fig. 3. High-resolution image of a polypropylene-polystyrene blend at a photon energy of 285.5 eV, where polystyrene is highly absorbing. Typically much smaller domains than in Fig. 2 are visible because of the action of a compatibilizer, which also improved the domain adhesion. The large polystyrene domain (**A**) had been exposed in its center to the focused beam for 80 min, without apparent morphological change or mass loss, whereas certain features (**B**) are a result of radiation damage that occurred after several minutes of exposure to the photon beam. The contrast and edge sharpness in this image is consistent with a Rayleigh resolution of 55 nm (300 × 300 pixels, 6 ms per pixel).

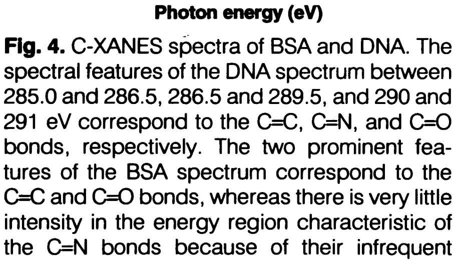

Fig. 4. C-XANES spectra of BSA and DNA. The spectral features of the DNA spectrum between 285.0 and 286.5, 286.5 and 289.5, and 290 and 291 eV correspond to the C=C, C=N, and C=O bonds, respectively. The two prominent features of the BSA spectrum correspond to the C=C and C=O bonds, whereas there is very little intensity in the energy region characteristic of the C=N bonds because of their infrequent occurrence in BSA (Table 1).

Although there is undoubtedly some radiation damage inflicted on the sample during imaging and acquisition of a spectrum, repeated images of the same sample area reveal no visible morphological changes or mass loss. To provide a more severe test of the radiation damage suffered by these polymer films during acquisition of data, we exposed the center of a polystyrene domain to the focused photon beam of 285.5 eV for 80 min, with no discernible mass loss or damage visible in the subsequent image (Fig. 3). This is to be compared to acquisition times of a few milliseconds per pixel to acquire an image and 5 s to acquire a spectrum of the quality shown in Fig. 1. However, polypropylene is less radiation-resistant than polystyrene. After exposures at a photon energy of 291.0 eV for a few minutes, which is over an order of magnitude longer than the time it takes for a spectrum, polypropylene showed mass loss on the order of a few percent. Upon a subsequent additional exposure of 15 min, the mass loss expanded to a ring-shaped pattern, whereas the center most heavily exposed to the beam showed a noticeable π^* resonance in the spectrum. The most appropriate comparison of the relative damage in organic specimens due to radiation inflicted by XANES spectroscopy and electron beam–based microscopes is that provided by EELS. EELS can be used to assess the same near-edge structure probed with XANES spectroscopy, but its electron beam generates more valence band transitions and secondary electrons per core hole than XANES spectroscopy does (*13*). Because most damage in organic materials is sustained by secondary electrons (*14*) and valence-band transitions, we can estimate that radiation damage in EELS is about three orders of magnitude larger than in XANES spectroscopy.

Because chemically specific images rely on absorption contrast between different features in the sample—just as regular imaging with the STXM—there is no penalty in spatial resolution incurred to achieve chemical contrast. Sections of predominantly carbon-based materials with densities close to 1 g/cm^3 can have thicknesses in the range of 40 to 800 nm to be suitable for C-XANES imaging. Thicknesses between 150 and 250 nm are optimal for good signal-to-noise ratios.

In biological specimens, there is a much wider variety of molecular environments than in the polymers presented here, leading to more complex XANES spectra. Proteins and nucleic acids, for example, all have carbon atoms double-bonded to oxygen, to nitrogen, and to other carbon atoms, which creates distinct π^* resonances. The relative frequencies of these double bonds, as shown in Table 1 for DNA and for a typical protein, bovine serum albumin (BSA), are characteristically different, providing a handle for spectroscopic identification. We prepared thin-film samples of these materials as standards. The observed spectra (Fig. 4) do exhibit the expected features, with the C=C and C=O resonances prominent for BSA, whereas DNA has a large integrated C=N intensity as well. To provide a demonstration of this contrast mechanism in a biological specimen, we prepared metaphase chromosomes, freeze-dried in 10 mM ammonium acetate, of the bean *V. faba*. The isolation procedures have been described elsewhere (*15*). Images of this specimen taken at photon energies of 281.3, 285.5, and 286.5 eV are shown in Fig. 5. On the basis of these images, the distribution of DNA can be determined (Fig. 5D); with a different set of images, the protein contribution could be determined as well. As observed by Kirtley *et al.*, there are characteristic spectral features in the

Table 1. Fractions of carbon double-bonded to the oxygen, nitrogen, and carbon atoms of BSA and four DNA bases (DNA) (*18*).

Molecule	Carbon atoms (*n*)	C=C	C=N	C=O
BSA	2935	0.077	0.014	0.243
DNA	39	0.103	0.154	0.103

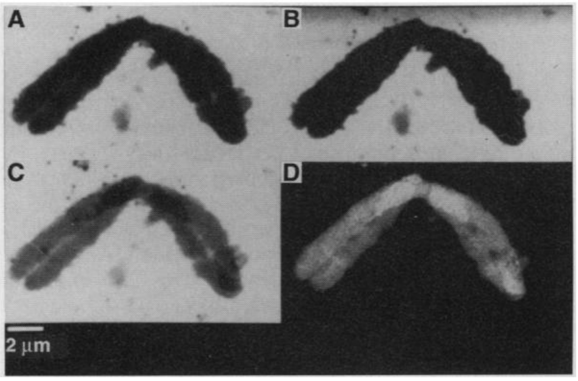

Fig. 5. Micrographs of metaphase chromosomes of the bean *V. faba* at the following photon energies: (**A**) 286.5 eV, (**B**) 285.5 eV, and (**C**) 281.3 eV. (**D**) The optical density distribution of DNA in the chromosomes, as computed from (B) and (C).

N-XANES spectra if the DNA bases are brominated (*2*). This sensitivity to bromine, and chemical labels with unique spectral signatures, should open up new possibilities in biological microscopy for functional and chemically specific imaging.

XANES spectroscopy provides excellent contrast for high-resolution imaging with chemical specificity. The ability to perform spectroscopy of organic materials $0.01\ \mu m^2$ in area and to form high-resolution images that use XANES contrast opens up new areas of study in structural biology and polymer science and in the investigation of other phase-separated materials. Here, we assumed a random, isotropic distribution of the molecules investigated. If explored with a suitable sample or sample rotation stage, the polarization dependence of XANES spectroscopy (*16*) would make it possible for researchers using our technique to determine the direction of specific bonds in oriented systems at high spatial resolution. The possibilities to use chemically specific labels in biology that have unique spectral signatures are particularly intriguing.

REFERENCES AND NOTES

1. R. D. Leapman and S. B. Andrews, *J. Microsc.* **165**, 225 (1992); P. M. Briber and F. J. Khoury, *J. Polym. Sci. Polym. Phys. Ed.* **26**, 621 (1988); L. Reimer, *Transmission Electron Microscopy* (Springer-Verlag, Berlin, 1988).
2. S. M. Kirtley *et al.*, *Biochim. Biophys. Acta*, in press.
3. J. C. Solem and G. C. Baldwin, *Science* **218**, 229 (1982).
4. J. C. Solem and G. F. Chapline, *Opt. Eng.* **23**, 193 (1984).
5. Related EELS spectra of nucleic acids can be found in M. Isaacson [*J. Chem. Phys.* **56**, 1813 (1972)].
6. H. Rarback *et al.*, *J. X-ray Sci. Technol.* **2**, 273 (1990).
7. E. Anderson and D. Kern, in *X-ray Microscopy III*, A. Michette, G. Morrison, C. Buckley, Eds. (Springer-Verlag, Berlin, 1992).
8. C. Jacobsen *et al.*, *Opt. Commun.* **86**, 351 (1991). Although the Rayleigh resolution of our instrument is 55 nm, features smaller than 36 nm have been resolved in test patterns.
9. This corresponds to the first minimum of the modified Airy pattern of our microprobe and contains 59% of the beam intensity.
10. S. J. Wu, *J. Polym. Sci. Polym. Phys. Ed.* **21**, 699 (1983).
11. S. Wu, *Polym. Eng. Sci.* **27**, 335 (1987); S. Cimmino *et al.*, *ibid.* **24**, 48 (1984).
12. S. Wu, *Polymer* **26**, 1855 (1987); R. J. M. Borggreve, R. J. Gaymans, J. Schuijer, J. F. Ingen Housz, *ibid.* **28**, 1489 (1987).
13. J. Cazaux, *Appl. Surf. Sci.* **20**, 457 (1985).
14. P. E. Laibinis, R. L. Graham, H. A. Biebuyck, G. M. Whitesides, *Science* **254**, 981 (1991).
15. S. Williams *et al.*, *J. Microsc.*, in press.
16. J. Stöhr, *NEXAFS Spectroscopy and the Structure of Adsorbed Molecules*, vol. 25 of Springer Series in Surface Science (Springer-Verlag, Berlin, 1992).
17. We used a fourth-order Butterworth filter with a cut-off at 40 cycles for the spectrum with 512 data points.
18. K. Hirayama, A. Satoko, M. Furuya, K. Fukuhara, *Biochem. Biophys. Res. Commun.* **173**, 639 (1990).
19. We are grateful to the many people who have contributed to this work. We particularly thank P. Stevens, who brought the possibilities of C-XANES spectroscopy to our attention. E. Anderson, D. Attwood, and D. Kern provided the zone plate, M. Rivers has been responsible for the data acquisition programs, C. Jacobsen helped implement the XANES acquisition mode, and C. Buckley, C. Jacobsen, S. Lindaas, H. Rarback, and S. Rock made important contributions to STXM development. The polymer samples were prepared by E. Berluche, S. Behal, J. Chludzinski, and S. McCarthy. Supported in part by NSF grant DIR 9005893. This work was performed at the National Synchrotron Light Source, which is supported by the Department of Energy, Office of Basic Energy Sciences.

29 May 1992; accepted 16 September 1992

The Age of Paraná Flood Volcanism, Rifting of Gondwanaland, and the Jurassic-Cretaceous Boundary

Paul R. Renne, Marcia Ernesto, Igor G. Pacca, Robert S. Coe,
Jonathon M. Glen, Michel Prévot, Mireille Perrin

The Paraná-Etendeka flood volcanic event produced ~1.5 × 10^6 cubic kilometers of volcanic rocks, ranging from basalts to rhyolites, before the separation of South America and Africa during the Cretaceous period. New ^{40}Ar/^{39}Ar data combined with earlier paleomagnetic results indicate that Paraná flood volcanism in southern Brazil began at 133 ± 1 million years ago and lasted less than 1 million years. The implied mean eruption rate on the order of 1.5 cubic kilometers per year is consistent with a mantle plume origin for the event and is comparable to eruption rates determined for other well-documented continental flood volcanic events. Paraná flood volcanism occurred before the initiation of sea floor spreading in the South Atlantic and was probably precipitated by uplift and weakening of the lithosphere by the Tristan da Cunha plume. The Paraná event postdates most current estimates for the age of the faunal mass extinction associated with the Jurassic-Cretaceous boundary.

Continental flood volcanism produces prodigious extrusions of chiefly basalt composition that in several cases exceed a volume of 1 × 10^6 km^3 (*1–3*). At least eight episodes of continental flood volcanism have occurred over the last 250 million years (My), and considerable attention has been devoted to understanding their genesis and relation to a variety of other terrestrial phenomena including hot spots, crustal rifting, and faunal mass extinctions. Detailed dating of several flood volcanic provinces (for example, the Deccan Traps, Siberian Traps, and Columbia River Basalts) has shown that one of the most distinctive features of flood volcanism is a very brief duration of principal activity that lasts 1 or 2 My at most, so that mean eruption rates are on the order of 10^6 km^3/My (*1–3*).

In this paper, we report new ^{40}Ar/^{39}Ar geochronologic data on the age and duration of volcanism in the Paraná province, one of the largest known continental flood volcanic provinces. These new data allow evaluation of the temporal relation between Paraná volcanism and the opening of the southern Atlantic Ocean and the Jurassic-Cretaceous mass extinctions.

Connections between flood volcanism, mantle plumes, hot-spot activity, and continental rifting were postulated over 20 years ago (*4*), and several contrasting genetic models for continental flood volcanic events have since emerged. Most models postulate that mantle plumes are responsible (*1–4*) but differ in whether decompression melting of the asthenosphere upon rifting above a preexisting mantle plume generates flood volcanism or, conversely, whether the rise of a mantle plume causes flood volcanism and initiates lithospheric extension (*1–3*). The imprecision in dating of some flood basalt events and associated rifting episodes has precluded confident deduction of their temporal sequence and hence their genetic relations.

A genetic link between flood volcanism and major faunal mass extinctions has been debated vigorously for nearly a decade (*5*), particularly with respect to the Deccan Traps of India and the Cretaceous-Tertiary (K-T) mass extinctions (*5, 6*). Recent dating of the Siberian Traps (*7, 8*) showed that this largest known continental flood volcanic province coincided within uncertainties with the most profound mass extinction event known at the Permian-Triassic boundary ~249 Ma (million years ago). The assessment of further coincidence of

---

P. R. Renne, Institute of Human Origins Geochronology Center, 2453 Ridge Road, Berkeley, CA 94709.
M. Ernesto and I. G. Pacca, Instituto Astrônomico e Geofísico, Universidade de São Paulo, 05508 São Paulo, Brazil.
R. S. Coe and J. M. Glen, Department of Earth Sciences, University of California, Santa Cruz, CA 95064.
M. Prévot and M. Perrin, Centre Geologique et Geophysique, 34060 Montpellier Cedex, France.